Therapeutic effects of exosome-based hyperin delivery in a cyclophosphamide-induced mouse model of diminished ovarian reserve

YI YING[1*], YUE WU[2*], JI ZHOU[1], YAMING WANG[3], HONGTAO YIN[4], GANG LU[5], RUOLANG PAN[5] and LIANGZHONG LV[2]

[1]Department of Traditional Chinese Medicine, Xianju People's Hospital, Hangzhou Medical College, Taizhou, Zhejiang 317300, P.R. China; [2]Center for Clinical Pharmacy, Cancer Center, Department of Pharmacy, Zhejiang Provincial People's Hospital (Affiliated People's Hospital), Hangzhou Medical College, Hangzhou, Zhejiang 310014, P.R. China; [3]Department of Gynecology, Xianju People's Hospital, Hangzhou Medical College, Taizhou, Zhejiang 317300, P.R. China; [4]Department of Psychology and Human Development, Institute of Education, University College London, London, WC1E 6BT, UK; [5]Key Laboratory of Cell-Based Drug and Applied Technology Development in Zhejiang Province, Institute for Cell-Based Drug Development of Zhejiang Province, S-Evans Biosciences, Hangzhou, Zhejiang 311122, P.R. China

Received December 25, 2025; Accepted August 3, 2026

DOI: 10.3892/mmr.2026.14021

Abstract. The development of more effective and affordable strategies for the treatment of diminished ovarian reserve (DOR) is of notable importance due to its increasing prevalence in young patients and the limited efficacy of current clinical interventions in restoring fertility. The present study investigated the efficacy of umbilical cord-derived mesenchymal stem cell (UCMSC)-derived exosome-based hyperin delivery in ameliorating cyclophosphamide (CP)-induced DOR in mice, and elucidated the potential underlying mechanisms of resulting therapeutic benefits. Exosomes were isolated from UCMSCs and encapsulated with hyperin using ultrasonication. The DOR mouse model itself was established via treatment with CP; these model mice were then treated with hyperin, UCMSC-exosome controls or hyperin-encapsulated UCMSC-exosomes. After treatment, body weight, estrous cycles and general health were monitored. Ovarian tissues were evaluated histologically, and serum levels of anti-Müllerian hormone, follicle-stimulating hormone and estradiol were measured via enzyme-linked immunosorbent assay. Ovarian expression of the autophagy markers LC3 II, Beclin-1 and P62 was analyzed via western blotting. CP treatment led to a notable deterioration in general health, body weight and ovarian function, as evidenced by altered estrous cycles and reduced follicle counts. Treatment with hyperin-loaded UCMSC-exosomes resulted in improvements in body weight, the restoration of estrous cycles. Notably, compared with the model group, mice treated with hyperin-loaded UCMSC-exosomes demonstrated increased primordial follicle counts and decreased atretic follicle counts. Treatment with hyperin-loaded UCMSC-exosomes modulated autophagic activity within the ovaries, with reduced LC3-II and beclin-1 levels and increased P62 levels following treatment with hyperin-loaded UCMSC-derived exosomes. UCMSC-derived exosomes loaded with hyperin effectively mitigated the adverse effects of CP on ovarian function, potentially via the modulation of autophagic processes. These findings supported the therapeutic potential of engineered exosomes for treating DOR, highlighting a novel approach for fertility preservation and reproductive medicine.

Correspondence to: Dr Ruolang Pan, Key Laboratory of Cell-Based Drug and Applied Technology Development in Zhejiang Province, Institute for Cell-Based Drug Development of Zhejiang Province, S-Evans Biosciences, 181 Wuchang Road, Hangzhou, Zhejiang 311122, P.R. China
E-mail: panrl@zju.edu.cn

Professor Liangzhong Lv, Center for Clinical Pharmacy, Cancer Center, Department of Pharmacy, Zhejiang Provincial People's Hospital (Affiliated People's Hospital), Hangzhou Medical College, 158 Shangtang Road, Hangzhou, Zhejiang 310014, P.R. China
E-mail: lvliangzhong@126.com

*Contributed equally

Key words: exosomes, hyperin, diminished ovarian reserve, autophagy, mesenchymal stem cell

Introduction

Diminished ovarian reserve (DOR) is a prevalent condition that affects the female reproductive system and has attracted notable attention (1,2). This condition is characterized by a decrease in the quantity and quality of oocytes in the ovaries, resulting in symptoms such as irregular menstrual cycles, reduced menstrual flow and infertility (3-5). DOR affects 10-30% of female patients of reproductive age and has

been increasingly observed in younger individuals, thereby posing a notable challenge to fertility and overall patient well-being (6,7).

Research has indicated that various inherent and external factors contribute to DOR. Age is a primary determinant of this condition because the number of oocytes in the ovaries declines steadily with advancing age. Furthermore, the steady decline in oocyte quantity together with the accelerated rate of follicular atresia with advancing age jointly affect oocyte quality (8). Genetic anomalies also play a notable role in DOR by directly impeding follicular development and ovarian function (9). Chromosomal and genetic abnormalities have been shown to affect primordial germ cell generation, meiosis, follicle development and ovulation. Common abnormalities in DOR include structural defects in the X chromosome, translocations and aneuploidy (10). For example, genetic abnormality or mutations in fragile X mental retardation 1, growth differentiation factor 9 (GDF9), follicle-stimulating hormone receptor (FSHR), and estrogen receptor 1 (ESR1), along with dysregulation of their downstream encoded proteins, have been shown to directly impair granulosa cell proliferation, steroidogenesis, and follicle development, thereby contributing to DOR (11-14).

Furthermore, immune factors have been implicated in diminishing the ovarian reserve, with certain autoimmune conditions, including rheumatoid arthritis, Sjögren's syndrome and systemic lupus erythematosus, being closely associated with DOR (15,16). DOR is also associated with various environmental influences and the psychological well-being of individuals (17). The elucidation of the pathogenic mechanisms related to DOR has advanced over the past two decades, along with marked progress in biological research techniques. However, targeted prevention and management strategies for DOR cases of unknown etiologies remain challenging (1,2).

Assisted reproductive technology is widely recognized in clinical practice as a viable treatment for patients with DOR seeking to conceive (18). Although ovulation induction methods can increase the number of retrieved oocytes and improve clinical pregnancy rates, the success rate tends to be lower in individuals with subpar oocyte quality. As such, hormone replacement therapy combined with oocyte donation and embryo transfer is viewed as a practical option for patients with poor oocyte quality (19). Additionally, adjunctive therapeutic agents, such as growth hormones and dehydroepiandrosterone, exhibit considerable potential for enhancing fertility outcomes (20,21). Stem cell (SC) therapy has garnered notable interest for use in DOR therapy due to its potential to repair damaged cells and stimulate cell proliferation, thereby demonstrating notable promise for restoring ovarian function and fertility in patients with DOR (22). Notably, mesenchymal SCs (MSCs) can promote the proliferation of ovarian GCs and inhibit GC apoptosis, thereby aiding the restoration of ovarian reserve function (23). However, stem cell therapy remains in the early stages of research; thus, further clinical studies and long-term safety and symptom monitoring are necessary to assess its safety and effectiveness.

Hyperin is a flavonol glycoside compound extracted from natural plants, such as *Cuscuta chinensis*, that has previously been investigated for its antioxidative, anti-apoptotic, anti-aging and immune-regulatory properties (24). However, the potential therapeutic effect of hyperin on ovarian reserve function or follicular development remains largely unexplored (25-27). The present study isolated exosomes from human umbilical cord-derived MSCs (UCMSCs) and used them to encapsulate hyperin via ultrasonic technology. The efficacy of hyperin treatment was then investigated in a mouse model of cyclophosphamide (CP)-induced DOR, and the potential mechanisms underlying hyperin-mediated therapeutic effects were explored.

Materials and methods

Cell lines and culture conditions. Human UCMSCs were provided by S-Evans (Hangzhou Yiwensai Biotechnology Co., Ltd.) as primary cells at passage 2. Upon receipt, the cells were thawed, cultured and expanded for three sequential passages in αMEM (Sigma-Aldrich; Merck KGaA) supplemented with 10% fetal bovine serum (FBS; Gibco; Thermo Fisher Scientific, Inc.) in a humidified atmosphere (95% relative humidity) at 37˚C with 5% CO_2, as reported in a previous study (28). The identification of UCMSCs in passage 5 was accomplished by performing morphological examinations, detecting the expression of surface markers and evaluating mesenchymal trilineage differentiation potential (osteogenic, adipogenic and chondrogenic) according to the minimal criteria defined by the International Society for Cellular Therapy (29). UCMSCs in passage 5 were also used in subsequent studies. KGN cells, which represent a human ovarian granulosa tumor cell line, were purchased from Applied Biological Materials Inc. (abm) (cat. no. T9195) and were cultured in DMEM (Sigma-Aldrich; Merck KGaA) supplemented with 10% FBS (Gibco; Thermo Fisher Scientific, Inc.) in a humidified atmosphere at 37˚C with 5% CO_2.

Antibodies and reagents. Antibodies against Beclin-1(cat. no. ab207612), LC3 II (ab192890) and P62 (ab109012) were purchased from Abcam, and anti-β-actin (AF0003) antibodies were obtained from Beyotime Biotechnology. Antibodies against CD63 (67605-1-Ig), CD9 (20597-1-AP), CD81(66866-1-Ig) and TSG101(28283-1-AP) were purchased from Proteintech. Hyperin was purchased from Sigma-Aldrich (cat. no. 83388, Merck KGaA). CP (PHR1404) was purchased from Merck KGaA.

Flow cytometry detection of surface markers. For surface marker detection, UCMSCs ($1x10^5$ cells/tube) were harvested, washed with ice-cold PBS (0.01 M, PH 7.4). Cells were blocked with 1% bovine serum albumin (BSA; Sigma-Aldrich; Merck KGaA) in PBS for 20 min at 4˚C and incubated with FITC- and PE (phycoerythrin-conjugated primary antibodies against CD73 (561014), CD90 (PE-conjugated; 561970), CD105 (568552), CD19 (PE-conjugated; 555413), CD45 (PE-conjugated; 555483) and human leukocyte antigen-DR (HLA-DR) (FITC-conjugated; 555811) (all 1:100; Waters Biosciences) for 30 min at 4˚C in the dark. Cells were washed twice and analyzed using a FACSCalibur™ flow cytometer (Waters Biosciences) and FlowJo software version 10.6.2 (FlowJo LLC).

Staining for cell differentiation. Primarily, multi-lineage differentiation was induced by transitioning UCMSCs at 90-95% confluence to specific induction media [HUXUC-90021,

HUXUC-90031, HUXUC-90041 for osteogenic, adipogenic and chondrogenic differentiation, respectively; Cyagen Bioscience (Suzhou), Inc.] in a humidified atmosphere (95% relative humidity at 37˚C with 5% CO_2. For osteogenic differentiation, cells were cultured for 3 weeks and fixed with ice-cold 4% paraformaldehyde for 15 min, followed by staining with 2% Alizarin Red S (OriCell) for 10 min at room temperature to visualize calcium deposits. For adipogenic differentiation, cells were induced for 2 weeks, fixed with 4% paraformaldehyde for 15 min at room temperature, followed by staining with 0.3% Oil Red O working solution (OriCell) for 15 min at room temperature to identify lipid droplets. For chondrogenic differentiation, high-density micromass cultures were maintained for 3 weeks, fixed with 4% paraformaldehyde for 15 min at room temperature, followed by staining with 1% Alcian blue (OriCell) for 30 min at room temperature to detect sulfated proteoglycans. Images were captured using an inverted light microscope (Olympus IX73; Olympus Corporation).

Exosome isolation. The αMEM containing 10% FBS was centrifuged at 100,000 x g for 10 h at 4˚C to eliminate any presence of bovine exosomes. Subsequently, the processed media underwent filtration using a 0.22 μm polyethersulfone syringe filter (cat. no. SLGPR33RS, Millipore; Merck KGaA) before being used for UCMSC culture. After UCMSCs were cultured in the exosome-depleted media for 48 h at 37˚C, the cell conditioned supernatants (containing secreted exosomes) were gathered and initially subjected to centrifugation at 800 x g for 10 min at a temperature of 4˚C to remove intact cells and cellular debris. The exosomes were isolated exclusively using the standard ultracentrifugation procedure. Briefly, the cell-conditioned media were sequentially centrifuged at 2,000 x g for 20 min at 4˚C and 10,000 x g for 30 min at 4˚C to eliminate cellular debris and large vesicles. The supernatants were then subjected to ultracentrifugation at 100,000 x g for 70 min at 4˚C using an Optima L-90K ultracentrifuge (Beckman Coulter, Inc.). The exosome pellets were washed with sterile PBS and ultracentrifuged again at 100,000 x g for 70 min at 4˚C for purification. The exosome pellets were suspended in PBS or saline solution; subsequently, a 20 μl aliquot of exosomes were lysed in RIPA buffer (P0013B, Beyotime Biotechnology) to determine their protein content using a BCA protein assay kit.

Hyperin was encapsulated into UCMSC-derived extracellular vesicles (EVs) using ultrasonication. Briefly, 200 μl hyperin solution was mixed with 200 μl of exosome suspension in a 1.5-ml microcentrifuge tube. The mixture was subjected to five cycles of ultrasonication on ice (each cycle consisting of 30 sec on and 90 sec off). Following ultrasonication, the mixture was incubated on a constant-temperature shaker at 37˚C for 1 h to allow membrane recovery. Unencapsulated free hyperin was removed by ultracentrifugation, and the drug-loaded exosomes (designated as EV-H) were resuspend in PBS and stored at 4˚C for subsequent assays. The drug encapsulation efficiency (EE%) of exosomes was calculated following UPLC-Q-TOF using the following equation: EE%=(amount of encapsulated hyperin/initial amount of hyperin added) x100%. The influence of drug loading on EV size was analyzed using nanoparticle tracking analysis (NTA). Briefly, exosome samples were diluted in particle-free PBS to achieve an optimal concentration range ($1x10^8$-$1x10^9$ particles/ml). NTA was performed using a ZetaView® PMX 120 analyzer (MicroTrac) equipped with a 488 nm laser. Videos of 60 sec durations were recorded at 11 positions at room temperature, and data were analyzed using ZetaView software version 8.05.12 (Microtrac MRB) to determine the particle size distribution profile. For stability evaluation, EV-Hs were incubated in PBS, 10% mouse serum [36118ES08; Yisheng Biotechnology (Shanghai) Co., Ltd.] or 50% mouse serum at 37˚C for 72 h. The retained ratio of hyperin in EV-Hs was measured to assess vesicular stability.

For cellular uptake tracking, isolated exosomes were labeled with the green fluorescent lipophilic dye PKH67 (Sigma-Aldrich; Merck KGaA) according to the manufacturer's instructions. PKH67-labeled exosomes (20 μg/ml) were incubated with KGN cells in three treatment groups [Control, control EV (EV-C) and hyperin-loaded EV (EV-H) groups] for 12 h at 37˚C. Following incubation, cells were washed with PBS, fixed with 4% paraformaldehyde for 15 min at room temperature, and counterstained with DAPI for 5 min at room temperature in the dark to visualize cell nuclei. Fluorescence signals were visualized and captured using a fluorescence microscope (Olympus IX73; Olympus Corporation).

Animal experiments. A total of 60 female specific pathogen-free-grade C57BL/6 mice aged 12 weeks (weight, 18-22 g) were purchased from the Laboratory Animal Center of Hangzhou Medical College. All mice were housed in an air-conditioned, SPF-grade animal room at a temperature of 22±2˚C and a relative humidity of 50-60% with a 12-h light/dark cycle and free access to water and chow. All experimental procedures were performed according to the National Institutes of Health Guidelines for the Care and Use of Laboratory Animals (30) and were approved by the Medical Animal Experiment Ethics Committee of the Hangzhou Medical College Laboratory Animal Center (Hangzhou, China; approval no. ZJCLA-IACUC-20050016).

Mice were randomly divided into five treatment groups: i) A control group; ii) a CP-induced DOR model group; iii) oral administration (OA) group, comprising DOR model mice that were orally administered hyperin; iv) a control EV (EV-C) group, comprising DOR model mice injected with empty exosomes; and v) a hyperin-loaded EV (EV-H) group, comprising DOR model mice injected with hyperin-loaded exosomes (n=12 per group). The OA group received intragastric administration of hyperin once every other day at 4 mg/kg/d. The EV-C and EV-H groups received intraperitoneal injections of 100 μl exosomes once every other day. A total of 1 week after hyperin treatment was initiated, all DOR model groups received intraperitoneal injections of CP solution at a weekly dose of 100 mg/kg; mice in the control group received an equal volume of saline via intraperitoneal injection. After 3 weeks of CP treatment, six mice in each group underwent euthanasia via prolonged exposure to 5% isoflurane for 3-5 min, which was administered via inhalation until cardiac arrest was confirmed. Following blood sampling and sacrifice, the bilateral ovaries of each mouse were harvested, trimmed of fat, and weighed. The ovarian index was calculated using the following formula: Ovarian index=[ovarian wet weight (mg)/body weight (g)] x100%, as previously described (31).

The remaining mice were kept on a normal diet for 2 weeks, after which these mice were paired with fertile male C57BL/6 mice (age, 12 weeks; body weight, 22-28 g; housed under the aforementioned conditions) at a female-to-male ratio of 2:1 for another 2 weeks to assess pregnancy status. Successful mating and pregnancy status were assessed by checking daily at 7:00 am for the presence of vaginal plugs (designated as embryonic day 0.5), and confirmed by subsequent gestational weight monitoring, conception time, and litter delivery. Following the completion of the breeding and fertility assessment, all mice were humanely euthanized using the identical protocol. None of the animals were reused for other subsequent experiments. Humane endpoints were pre-established to minimize animal suffering. All mice were monitored daily for clinical signs of distress, and mice were scheduled for immediate mandatory early euthanasia upon meeting the following criteria: i) Severe weight loss (>20% of baseline); ii) prolonged and unrecoverable lethargy or unresponsiveness to stimulation; iii) intractable hunched posture with inability to obtain food or water; or iv) acute pain. Although mild, transient clinical signs of CP-induced toxicity, such as dull coat and mild hunching, were observed in the model groups, no mice reached the threshold for severe, irreversible distress requiring early humane endpoint intervention.

Serum preparation and enzyme-linked immunosorbent assay (ELISA). The mice underwent a 12-h fasting period before being euthanized. Blood was obtained from the retrobulbar venous plexus as a terminal procedure after inducing deep anesthesia using 5% isoflurane inhalation. An average volume of 0.4-0.5 ml whole blood was collected from each mouse. A pyrogen and endotoxin-free centrifuge tube was used for blood collection, and blood samples were subsequently incubated at room temperature for 30 min. Following incubation, blood was centrifuged at 1,000 x g for 10 min at 4˚C to separate the light-yellow serum layer from other blood contents; this layer was then carefully aspirated, transferred into a cryovial and stored at -80˚C for future use. ELISA kits were later used to detect the serum levels of anti-Müllerian hormone (AMH) (ml037597), FSH (ml001910, mlbio) and estradiol (E2) (ml001962; all Shanghai Enzyme-linked Biotechnology Co., Ltd.).

Analysis of mouse estrous cycle. To track estrous cycle dynamics, vaginal cytological smears were collected once daily throughout the 28-day treatment period across all experimental groups. Every morning at 8:00 am, a sterilized cotton swab was moistened with physiological saline and inserted into the vagina to a depth of ~0.5 cm. The swab was gently rotated to collect secretions, which were then evenly applied onto a glass slide and allowed to dry. An appropriate amount of ice-cold 4% paraformaldehyde was added in a dropwise manner to secretions for post-fixation lasting 15 min. Subsequently, microscope slides were stained with hematoxylin for 5 min, differentiated using hydrochloric acid and alcohol for 10 sec, stained with eosin for 20 sec at room temperature and rinsed with running water thoroughly before the slides were dried and sealed. The morphology of exfoliated cells was examined under a light microscope to determine the estrous-cycle stage of each sample. Estrous stages were characterized as follows: i) Samples from mice in diestrus showed numerous white blood cells and minimal mucus; ii) samples from mice in proestrus displayed abundant nucleated epithelial cells alongside few keratinized epithelial cells; iii) samples from mice in estrus presented with predominantly keratinized epithelial cells, and also contained a number of nucleated epithelial cells; and iv) samples from mice in late estrus consisted primarily of nucleated epithelial cells accompanied by leukocytes and small amounts of keratinized epithelial cells as previously reported (32,33).

Cell treatment and assessments of mitochondrial membrane potential. KGN cells were harvested during the log-phase of growth and seeded at a density of $3x10^5$ cells/ml. Cells were subsequently randomly divided into four groups; for two of these groups, cells were pre-treated with 100 μl EV-C and EV-H, respectively for 48 h at 37˚C. Subsequently, 10 μM 4-hydroperoxycyclophosphamide (4-HC) was added to each group of cells for additional 24 h. Since 4-HC was dissolved in DMSO for storage, an equivalent concentration of DMSO was added to the control group to rule out solvent interference. Autophagy levels in KGN cells were evaluated by measuring LC3 II, P62 and Beclin 1 protein expression via western blotting.

According to the manufacturer's instructions, mitochondrial membrane potential was assessed using the JC-10 Mitochondrial Membrane Potential Assay Kit for flow cytometry (Abcam) and microplate assays (Abcam). For flow cytometry analysis, $1x10^6$ cells were harvested and suspended in 1X JC-10 dye-loading solution at a volume of 500 μl, incubated at room temperature for 30 min and subsequently analyzed via channels for green-fluorescent monomeric and orange-fluorescent aggregate signals using a FACSCalibur™ flow cytometer (Waters Biosciences) and FlowJo software version 10.6.2 (FlowJo LLC). For microplate assays, cells were placed in a 96-well plate and exposed to 50 μl aliquots of JC-10 dye-loading solution at 37˚C for 30 min. Subsequently, the fluorescence intensities of aggregates and monomeric forms of JC-10 were measured using a Synergy H1 microplate reader (BioTek; Agilent Technologies, Inc.) with excitation/emission wavelengths of 490/530 and 490/590 nm after the addition of assay buffer B (50 μl per well).

Hematoxylin and eosin (H&E) staining. Mouse ovarian tissue samples (n=3) were harvested and fixed in 4% paraformaldehyde at room temperature for 24 h prior to paraffin embedding. Paraffin-embedded tissue blocks were sliced into 5 μm-thick sections, with every 5th section collected for analysis. The sections were dewaxed with xylene, rehydrated through a descending ethanol series, stained with hematoxylin for 5 min at room temperature, rinsed with tap water and differentiated using 1% hydrochloric acid alcohol for 10 sec at room temperature. Subsequently, sections were rinsed again with tap water, stained with eosin for 20 sec at room temperature, dehydrated through ascending ethanol and cleared with xylene. Neutral gum was added to each section and the coverslips were sealed. Sections were observed and images were captured under light microscope (Olympus BX53; Olympus Corporation). Each section was evaluated and counted by the same experienced observer; primary and secondary follicles were classified as early-developing follicles, whereas primary, secondary and antral follicles were classified as developing follicles.

Western blot analysis. Total proteins were extracted from exosomes, mouse ovarian tissue or KGN cells using RIPA lysis buffer containing 1% PMSF (ST505, Beyotime Biotechnology), and protein concentration was measured using BCA protein assay. A total of 20 μg protein/lane was loaded into stacking gels and subsequently run through 10-12% SDS-PAGE at a voltage of 60 V. Electrophoresis was performed on a separation gel at 120 V. Proteins were transferred onto 0.45-μm PVDF membranes in an ice-water mixture using a constant current of 330 mA for 90 min. Membranes were blocked with 5% non-fat dried milk in TBST with 0.1%Tween-20 for 60 min at room temperature, followed by overnight incubation at 4˚C with the aforementioned primary antibodies (all 1:1,000). Membranes were incubated with horseradish peroxidase (HRP)-conjugated goat anti-rabbit (cat. no. A0208, Beyotime Biotechnology) or HRP-conjugated goat anti-mouse IgG (H+L) (both 1:5,000; A0216, Beyotime Biotechnology) secondary antibodies on a shaker at room temperature for 1 h on the following day. Immunoreactive proteins were visualized using an enhanced chemiluminescence detection kit (P0018S, Beyotime Biotechnology) and imaged with a chemiluminescent immunodetection system (ChemiDoc XRS+; Bio-Rad Laboratories, Inc.). ImageJ (National Institutes of Health, version 1.53) was used to analyze the grayscale values of protein bands using anti-β-actin as a housekeeping control.

Transmission electron microscopy (TEM) analysis. KGN cells were fixed in 2.5% glutaraldehyde at 4˚C for 4 h. Samples were then rinsed with PBS, dehydrated in solutions of increasing ethanol and subsequently embedded in epoxy resin at 60˚C for 48 h. Samples were sectioned at a thickness of 90 nm, stained with 1% uranyl acetate for 2 min at room temperature and lead citrate for 5 min at room temperature, and were subsequently examined using an transmission electron microscope (H-7650; Hitachi, Ltd.).

Ultra-performance liquid chromatography-quadrupole-time-of-flight (UPLC-Q-TOF) mass spectrometry analysis. Mouse serum samples were prepared for quantification of hyperin, with quercetin (100 ng/ml) added as an internal standard. Chromatographic separation was performed on an Agilent 1290 Infinity II LC system (Agilent Technologies, Inc.) using an Agilent ZORBAX Eclipse Plus C18 column (2.1x100.0 mm; particle size, 1.8 μm; Agilent Technologies, Inc.) maintained at 40˚C, while the autosampler was set at 4˚C. The mobile phase consisted of 0.1% (v/v) formic acid in water (solvent A) and acetonitrile (solvent B). The gradient elution profile was optimized as follows: 0-2 min, 10% solvent B; 2-7 min, 10-40% solvent B; 7-10 min, 40-95% solvent B; 10-12 min, 95% solvent B; and 12-15 min, 10% solvent B for column re-equilibration. The flow rate was maintained at 0.3 μl/min with an injection volume of 2 μl.

Mass spectrometry evaluation was conducted using an Agilent 6545 Q-TOF mass spectrometer (Agilent Technologies, Inc.) equipped with an electrospray ionization source operating in positive ionization mode. The mass spectrometry parameters were configured as follows: i) Capillary voltage, 3.5 kV; ii) gas temperature, 320˚C; iii) drying gas flow rate, 8 l/min; iv) nebulizer pressure, 35 psi; and v) fragmentor voltage, 135 V. Quantification was executed by monitoring the protonated molecular ion $[M+H]^+$ of hyperin at 465.10 m/z using Agilent MassHunter software version B.08.00 (Agilent Technologies, Inc).

Statistical analysis. All experiments were independently repeated ≥3 times. All data are presented as the mean ± standard deviation. Statistical differences among multiple groups were evaluated using one-way ANOVA followed by Tukey's post-hoc test in GraphPad 7.0 (Dotmatics). $P<0.05$ was considered to indicate a statistically significant difference.

Results

Hyperin can be effectively loaded in UCMSC-derived exosomes. UCMSCs were initially isolated and cultured up to passage 5 and subjected to morphological assessment, lineage differentiation and surface marker analysis. UCMSCs maintained their typical spindle-shaped morphology (Fig. 1A) and exhibited robust tri-lineage differentiation potential: osteogenic differentiation was confirmed by mineralized calcium deposits (Fig. 1B), adipogenic differentiation by intracellular lipid droplet accumulation (Fig. 1C) and chondrogenic differentiation by matrix glycosaminoglycan synthesis (Fig. 1D). Additionally, flow cytometry analysis demonstrated high expression of classical MSC positive surface markers CD73, CD90 and CD105, whereas hematopoietic markers, such as CD19, CD45 and HLA-DR, were absent (Fig. 1E), confirming the purity and identity of UCMSCs. These results suggested that UCMSCs met the criteria for standard MSC characteristics (26).

Exosomes were isolated from culture medium that was conditioned with UCMSCs for 48 h. NTA revealed comparable mean diameters for EV-Cs (119 nm) and EV-Hs; 120 nm). Transmission electron microscopy analysis provided evidence that the exosomes maintained their characteristic double-layered membrane structure (Fig. 1F), indicating that the ultrasonication effectively encapsulated hyperin without destroying the physical membrane integrity of the exosomes. Western blotting was subsequently used to assess the expression levels of marker proteins on the surface membrane of UCMSCs before and after drug-loading. The results demonstrated that the exosomal markers CD9, CD63, CD81 and TSG101 were positively expressed in both the EV-C and EV-H groups (Fig. 1G).

Based on the results of UPLC-Q-TOF, the concentration of hyperin in EV-Hs was 3.509±0.1923 nmol, whereas the concentration of free hyperin in the supernatant was determined to be 31.38±0.3413 nmol, indicating a drug-loading rate of ~10%. Additionally, no significant decrease in the drug-loading capacity of EV-Hs was observed within 24 h of drug loading at 4˚C, suggesting the feasibility of EV-H use in subsequent animal experiments (Fig. 1H). Furthermore, the stability of EV-Hs was evaluated in PBS, 10% mouse serum and 50% mouse serum. Analysis revealed that after 72 h incubation, the long-term stability of EV-Hs were 87.7±3.8% in PBS, 88.3±4.5% in 10% mouse serum, and 87.0±2.6% in 50% mouse serum (Fig. 1I). Subsequently, the uptake of exosomes by KGN cells was compared between the two groups via staining of exosomes. As shown in Fig. 1J, green fluorescent signals were observed in the cytoplasm of KGN

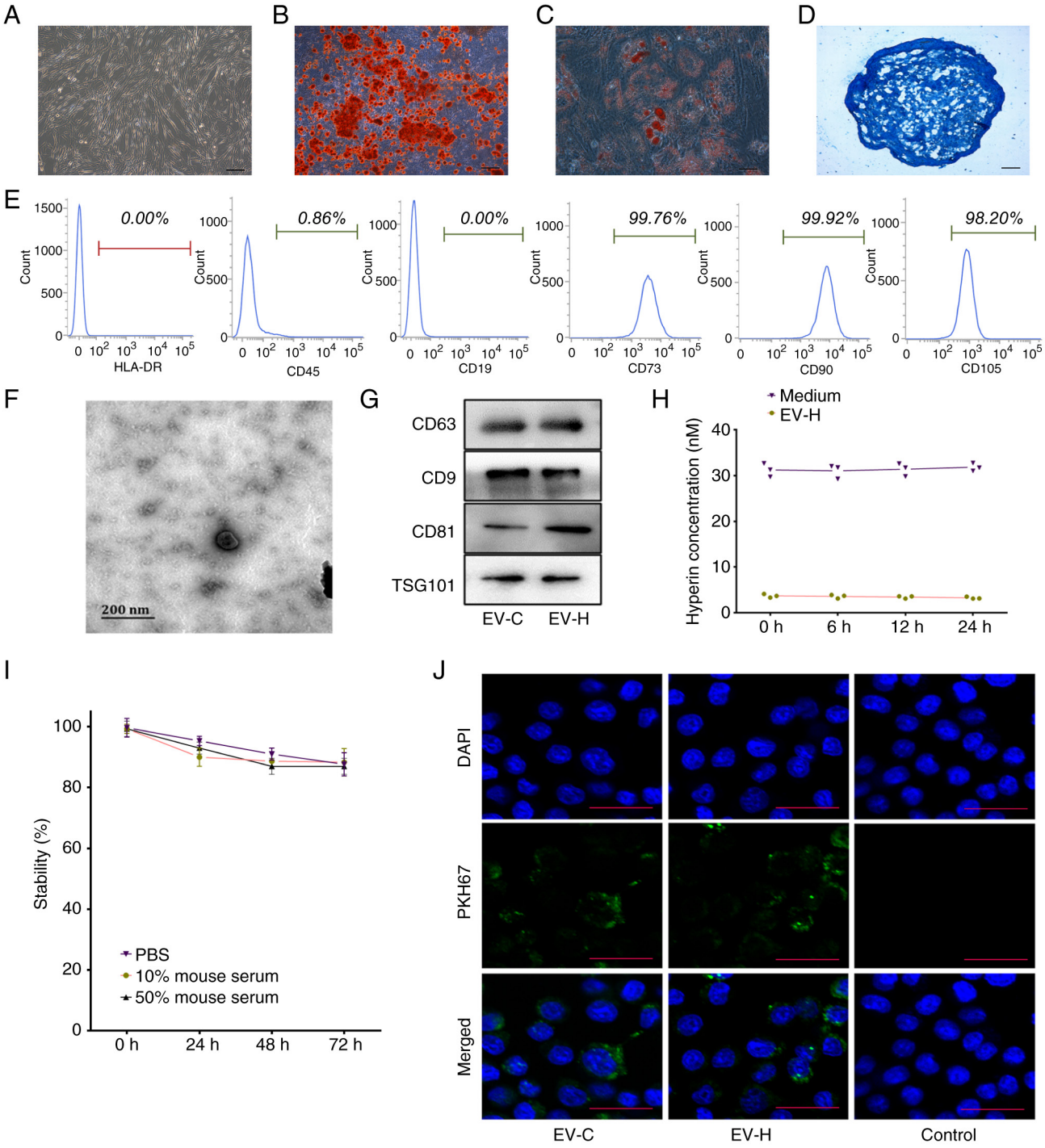

Figure 1. UCMSC-derived exosomes achieve effective hyperin drug delivery. (A) The morphology of UCMSCs in passage 5 reached 90% confluence (scale bar, 50 μm). Then, the culture medium was replaced with a specific lineage induction medium. Representative inverted light microscopic images showing cells 2-3 weeks post-lineage induction after staining with (B) Alizarin Red S, (C) Oil Red O and (D) Alcian blue (scale bar, 50 μm). (E) Flow cytometry results indicated that UCMSCs were positive for CD73, CD90 and CD105 and negative for CD19, HLA-DR and CD45. (F) Representative transmission electron microscopy image of hyperin-loaded exosomes (scale bar, 200 nm). (G) Western blot assays revealed the positive expression of typical exosome markers in UCMSC-derived exosomes. (H) Analysis of drug-loading capacity of UCMSC-derived exosomes indicated that the exosomal loading rate of hyperin was ~10% and remained stable within 24 h. (I) Analysis of stability of hyperin-loaded exosomes in PBS, 10 and 50% mouse serum. (J) Fluorescence microscopy was used to analyze the uptake of PKH67-labeled exosomes (green signals) in KGN cells, demonstrating that hyperin drug loading did not affect cellular internalization (scale bar, 50 μm). EV-C, control extracellular vesicle; EV-H, hyperin-loaded exosomes.

cells in both EV groups, indicating that hyperin drug loading did not notably affect the uptake of exosomes. Thus, the results showed that EVs could be used for drug-loading without their physical properties being altered and could deliver hyperin efficiently and stably to affected tissues for *in vivo* studies.

Exosome-based hyperin delivery reduces CP-induced DOR symptoms in mice. The present study then assessed whether hyperin could alleviate DOR symptoms in a murine model of the disease. As illustrated in Fig. 2A, healthy female mice were divided into five groups and administered different treatments.

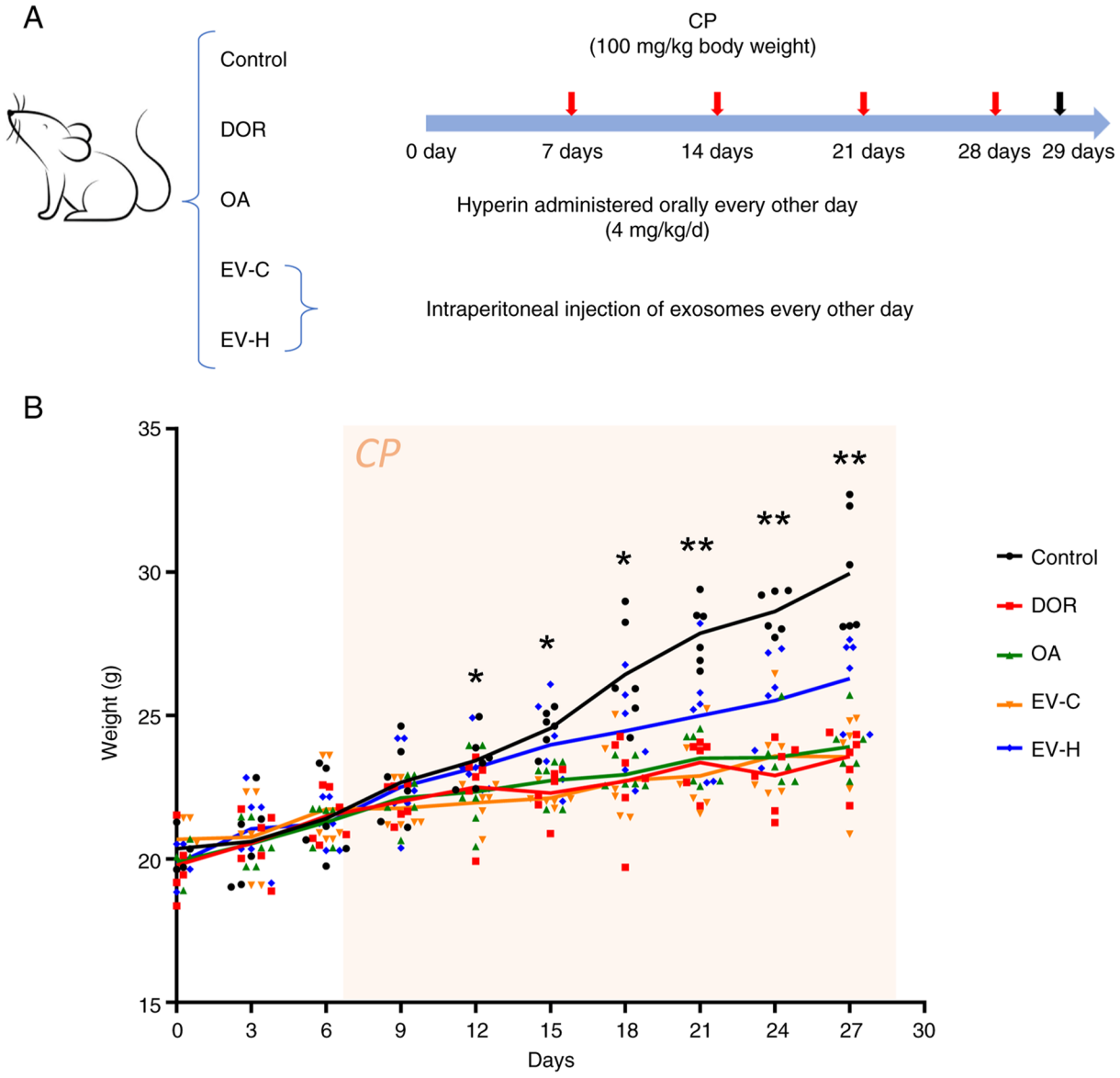

Figure 2. Evaluation of the therapeutic effect of hyperin on a CP-induced DOR mouse model. (A) Experimental schematic flow diagram, showing how mice were randomly assigned to five treatment groups: Control, DOR, OA, EV-C and EV-H groups. Therapeutic administration of hyperin was initiated on day 1 and performed once every other day. On day 7, a weekly dose of CP was administered to mice all groups except the control group via intraperitoneal injection to induce DOR-like pathology (red arrow). Mice were systematically monitored and a subset of mice were sacrificed on day 29 (black arrow). (B) Body weights of mice across the five treatment groups were recorded longitudinally at designated time points throughout the 4-week experimental period. *P<0.05 and **P<0.01, vs control. DOR, diminished ovarian reserve; CP, cyclophosphamide; OA, oral administration; EV-C, control extracellular vesicle ; EV-H, hyperin-loaded exosomes.

No mortality was observed in any group throughout the administration period prior to the experimental endpoint. Starting on day 21, mice in the DOR group exhibited mild clinical signs of CP-induced systemic discomfort, including a dull coat, hunched backs and reduced activity levels. However, none exhibited severe unresponsiveness or met the pre-established humane endpoints for early euthanasia, as mice maintained active grooming, preserved their righting reflex and maintained adequate food and fluid intake. The body weights of mice from all groups showed no significant differences during the first week (Fig. 2B). After receiving CP via intraperitoneal injection on day 7, the body weights of mice in the DOR, OA and EV-C groups increased slowly. Compared with the control group, the DOR group showed a significant reduction in body weight at all tested time points from day 12 onwards. The OA and EV-C groups did not exhibit any statistically significant differences when compared with each other or with the DOR group at any measured time points. Although visual markers, such as coat color, showed improvement in mice in the OA treatment group, mice exhibited decreased food intake, which may have been attributed to the higher dosage of hyperin administered via the intragastric method. Mice treated with EV-H demonstrated markedly higher levels of weight gain than those from the DOR, OA and EV-C treatment groups.

In addition, the present study simultaneously assessed changes in the estrous cycle of female mice across treatment groups, as shown in Fig. 3A. Before CP administration, all groups displayed a regular estrous cycle with relatively

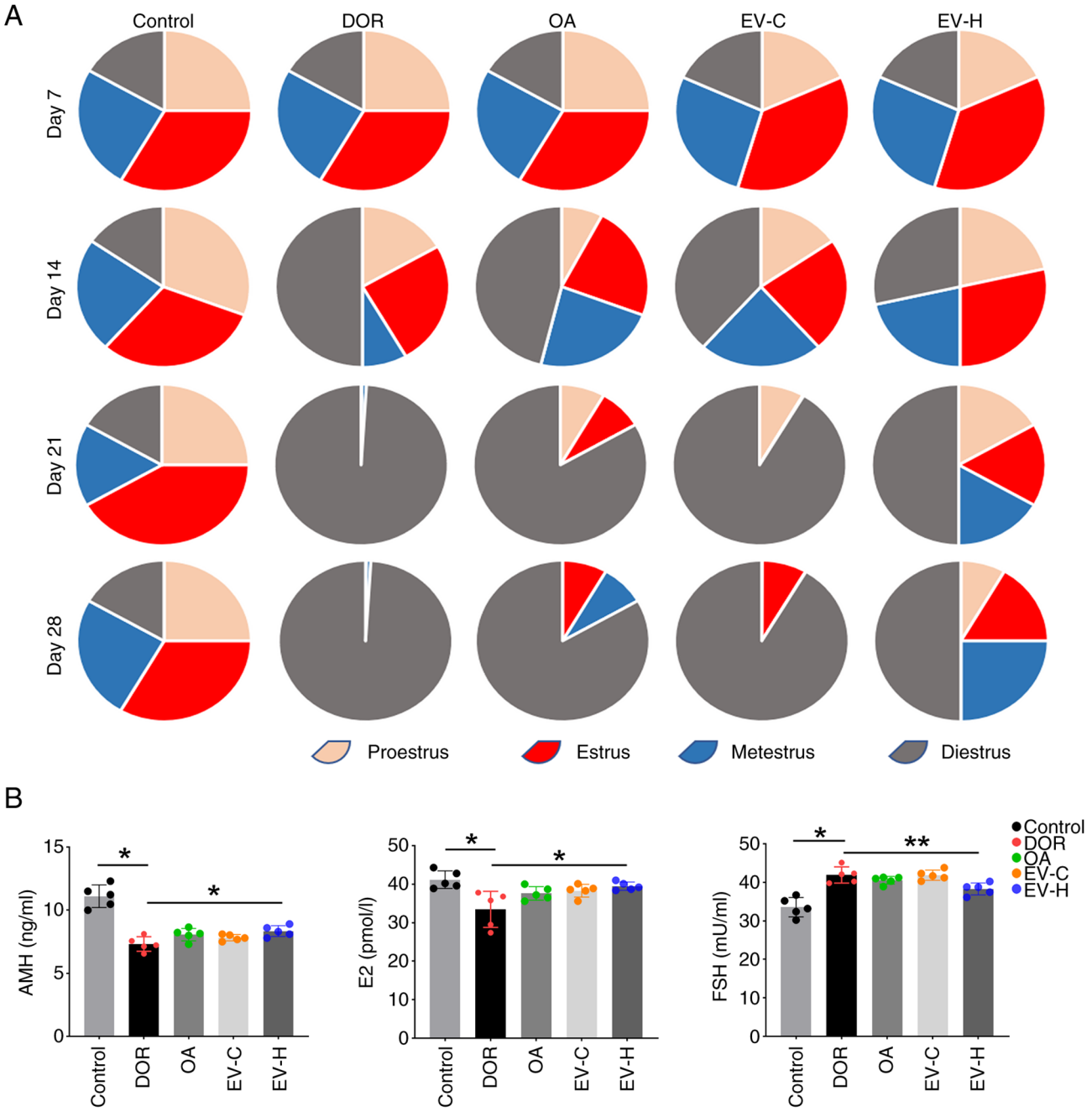

Figure 3. Detection of estrous cycle changes and sex hormone levels in mice of each group. (A) As the experiment progressed, changes in the proportion of mice in each stage of the estrous cycle were recorded across treatment groups. (B) By day 29, a subset of mice in each group were sacrificed. Hormone levels in the serum of each group of mice were detected and evaluated. *P<0.05 and **P<0.01. DOR, diminished ovarian reserve; OA, oral administration; EV-C, control extracellular vesicle; EV-H, hyperin-loaded exosomes ; AMH, anti-Müllerian hormone; E2, estradiol; FSH, follicle-stimulating hormone.

even stage distribution (Fig. S1). Subsequently, the diestrus phases gradually extended in the DOR group and these mice remained stagnant in diestrus for an extended period after 2 weeks of treatment. Mice from both the OA and EV-C groups showed notable disruptions in their estrous cycles following CP injection, with a notable prolongation of the estrus period; however, signs of estrus were consistently present during treatment. Comparison among these groups revealed a notable improvement in the estrous cycles of mice within the EV-H group; even after 3 weeks of CP treatment, EV-H-treated mice exhibited significant restoration of normal estrous cyclicity and regular stage transitions.

Mouse serum was collected on day 29 following the final observation to assess the AMH, FSH and E2 levels of mice in each group. As in Fig. 3B, analysis of mice in the DOR model group revealed a significant decrease in AMH and E2 levels compared with those in the control group, along with a significant increase in serum FSH levels. No notable differences in AMH, FSH and E2 levels were observed between the DOR model group and the OA or EV-C groups. However, compared with the DOR model group, a significant increase in AMH levels was observed in mice within the EV-H group. This increase was accompanied by a significant rise in E2 and a significant decrease in FSH levels, indicating

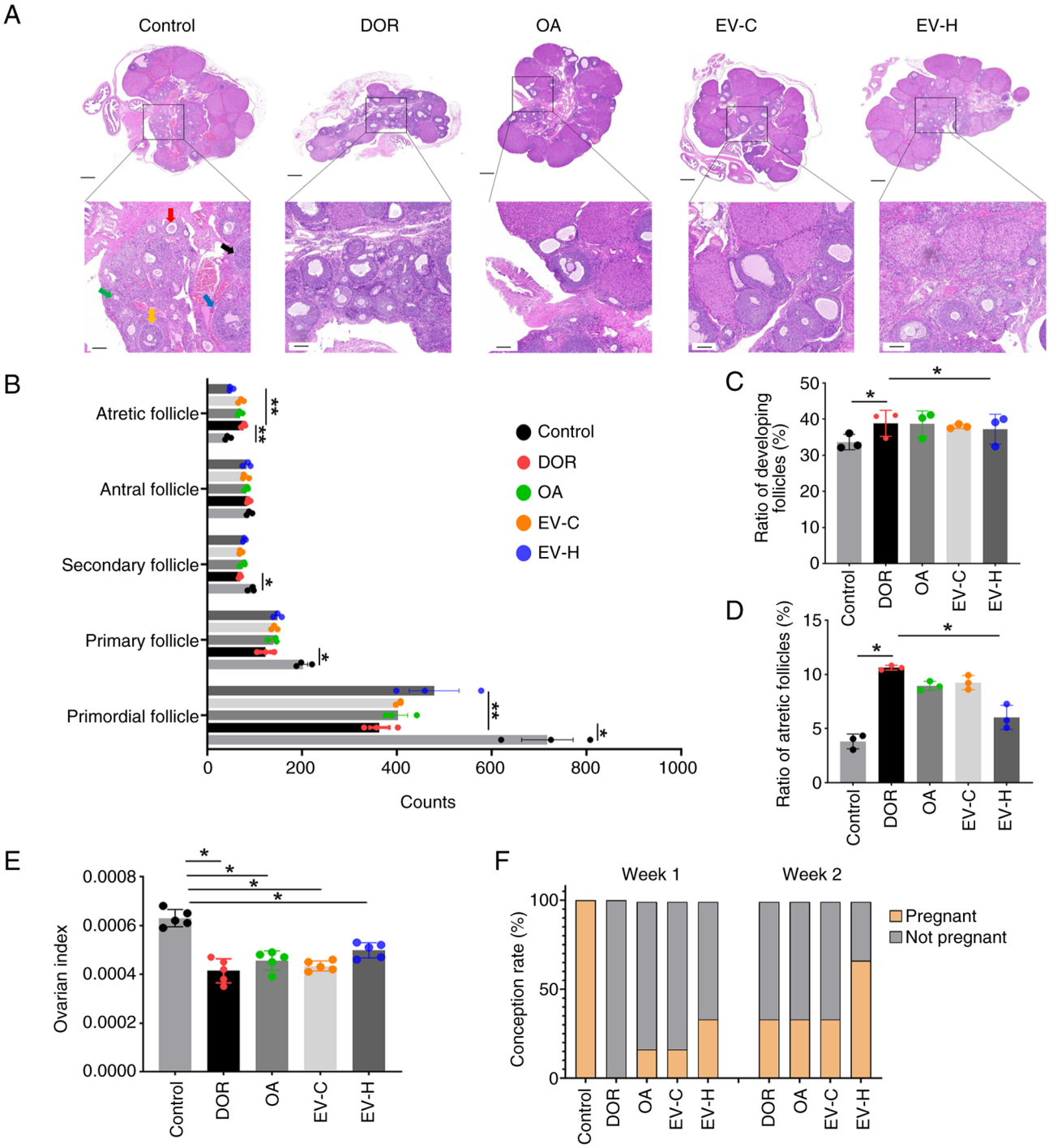

Figure 4. Delivery of hyperin via exosomes attenuates symptoms of cyclophosphamide-induced DOR in mice. (A) Representative images of hematoxylin and eosin staining of ovaries from mice in each treatment group (scale bar, 500 and 100 μm). Black arrow, atretic follicle, blue arrow indicated antral follicle, yellow arrow indicated secondary follicle, red arrow indicated primary follicle, and green arrow indicated primordial follicle. (B) Number of follicles of different grades in mice in each treatment group. (C) The proportion of developing follicles in each group. (D) The proportion of atretic follicles in each group. (E) Ovarian index of mice in each group. n=5. (F) Comparison of conception time of mice in each group. n=6. *P<0.05 and **P<0.01. DOR, diminished ovarian reserve; OA, oral administration; EV-C, control extracellular vesicle; EV-H, hyperin-loaded exosomes.

considerable improvements in hormone levels in DOR model mice following EV-H treatment.

As shown in Fig. 4A, ovarian follicles in all developmental stages were observed in mice from the healthy control group, featuring plump oocytes and abundant GCs in the antral follicles; furthermore, atretic follicles were sporadically observed. By contrast, mice from the DOR model group displayed a notable reduction in ovarian volume and a less dense ovarian stroma. Fig. 4B showed that, compared with the control group, the quantity of primordial, primary and secondary follicles decreased significantly in the DOR group, whereas the number of atretic follicles increased. No significant changes were observed in the number of antral follicles between these groups. Mice from the OA and EV-C groups showed notable

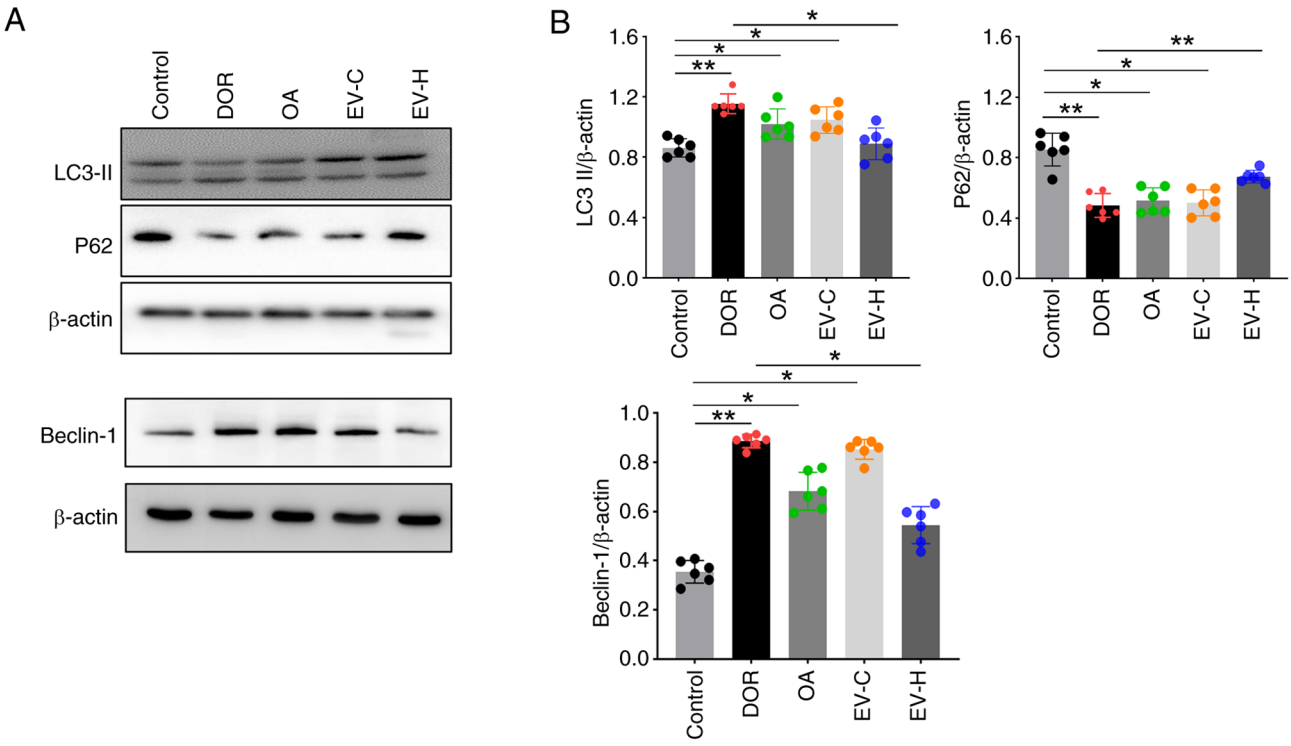

Figure 5. Expression of LC3-II, beclin-1 and P62 proteins in the ovaries of mice in each group. (A) Western blot assays were conducted to evaluate LC3-II, beclin-1 and P62 protein levels across treatment groups, and (B) grayscale values were semi-quantitative analyzed using ImageJ. β-actin was used as an internal reference. *P<0.05 and **P<0.01. DOR, diminished ovarian reserve; OA, oral administration; EV-C, control extracellular vesicle; EV-H, hyperin-loaded exosomes.

increases in ovarian volume, characterized by a less dense ovarian stroma and degenerated oocytes with sparse, apoptotic GCs. Compared with the control, the quantity of primordial, primary and secondary follicles decreased significantly in the DOR group, whereas the number of atretic follicles increased. No significant changes were observed in the number of antral follicles between these groups. Comparatively, mice in the EV-H group displayed marked histological protection, featuring well-preserved and compact ovarian stroma, healthy plump oocytes, and multiple layers of abundant, well-organized GCs.

Furthermore, no notable improvements in the numbers of other types of follicles or the number of atretic follicles in these groups was observed compared with the DOR group. Comparatively, mice in the EV-H group exhibited a significant increase in the absolute number of primordial follicles compared with those in the DOR group, whereas the absolute number of atretic follicles significantly decreased, demonstrating that EV-H effectively suppressed follicular atresia. CP treatment in DOR mice induced severe depletion of the primordial pool, resulting in an altered percentage distribution of developing follicles relative to total remaining follicles (Fig. 4C). EV-H administration effectively normalized the proportion of healthy developing follicles and significantly reduced the ratio of atretic follicles (Fig. 4D), demonstrating overall restoration of follicular pool composition. On day 29, concurrent with serum collection, the ovarian index of samples was evaluated (31). The ovarian index values of treated mice in each group were significantly decreased compared with that of the mice from the control group (Fig. 4E). Subsequently, to evaluate the fertility outcomes of each treatment, the remaining mice in each group were maintained on a regular diet for 2 weeks before being paired with fertile male C57BL/6 mice at a ratio of 2:1; Fig. 4F depicts the number of pregnancies in each group. A total of 7 days pf cohabitation, all 6 control group mice became pregnant, whereas none of the DOR group mice became pregnant. At this 1-week mark, 1 mouse each from the OA and EV-C groups was pregnant, whereas 2 EV-H group mice became pregnant. By day 14 of cohabitation, mice from the DOR, OA and EV-C groups demonstrated a pregnancy rate of 2 out of 6, whereas mice in the EV-H group exhibited a pregnancy rate of 4 out of 6. These findings demonstrated that EV-H administration notably improved ovarian follicle development and reduced follicular atresia and improved functional fertility in mice with CP-induced DOR.

Exosome-based hyperin delivery suppresses CP-induced autophagy both in vivo and in vitro. Subsequently, the present study investigated the levels of autophagy within the ovarian tissues of each group of mice. The differences in LC3-II, P62 and beclin-1 protein levels in each group, as detected by western blot analysis, are presented in Fig. 5. In the DOR model group, the expression levels of LC3-II and beclin-1 increased significantly compared with those in the control group, whereas the P62 protein expression decreased significantly. Similarly, compared with the control group, the OA and EV-C groups exhibited significant increases in LC3-II and Beclin-1 expression, along with a significant decrease in P62 expression. Notably, no significant difference in LC3II, P62 and Beclin-1 expressions was observed

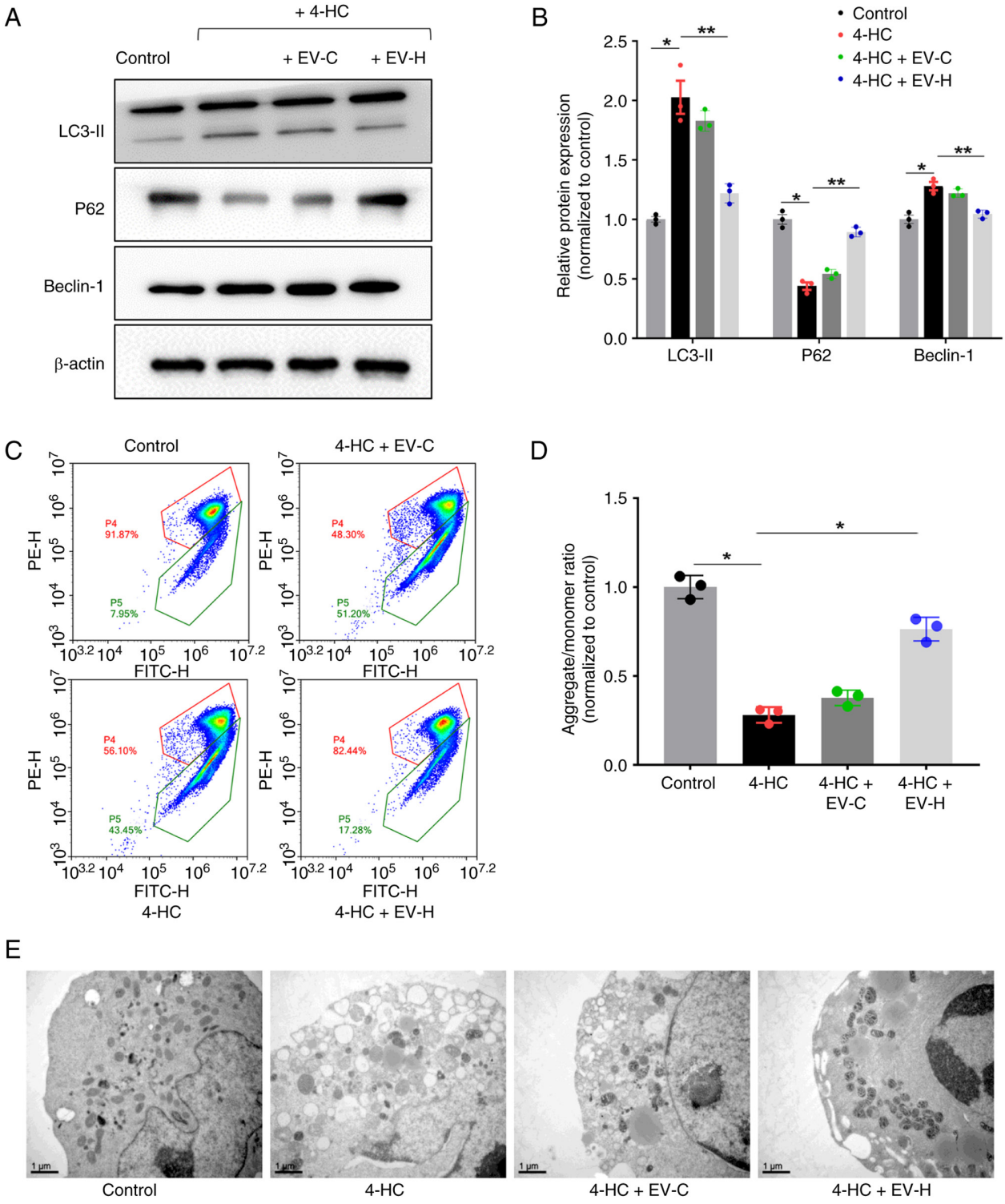

Figure 6. Exosome-based hyperin delivery inhibited 4-HC-induced autophagy in KGN cells. KGN cells were pre-treated with or without EV-C or EV-H for 48 h and then exposed to 10 μM 4-HC for 24 h. (A) Protein levels of autophagy markers, such as LC3-II, P62 and beclin-1, were detected by western blotting and (B) semi-quantitatively analyzed using ImageJ. Mitochondrial membrane potential was also assessed in different treatment groups via JC-10 staining followed by (C) flow cytometry and (D) microplate reader analysis. (E) Representative transmission electron microscopy images for detecting mitophagic vacuoles in KGN cells as signs of autophagy (scale bar, 1 μm). *P<0.05 and **P<0.01. 4-HC, 4-hydroperoxycyclophosphamide; EV-C, control extracellular vesicle; EV-H, hyperin-loaded exosome.

between the EV-H and control groups. Furthermore, compared with mice in the DOR model group, mice in the EV-H group exhibited significant decreases in the expression levels LC3-II and beclin-1 and a significant increase in P62 protein expression. These findings indicated that EV-H effectively inhibited CP-induced autophagy activation in mouse ovarian tissues.

Dysfunction of GCs, which represent the largest cell group in the ovarian follicle and are responsible for secreting steroid hormones and cytokines, has been shown to lead to follicular

atresia and may cause DOR (34). In the present study, the KGN ovarian GC line, was utilized for *in vitro* experiments and subject to treatment with 4-HC, the active metabolite of CP. As shown in Fig. 6A and B, exposure to 10 μM 4-HC for 24 h effectively triggered protein level alterations indicative of autophagic activation in KGN cells. A significant rise in LC3-II expression and beclin-1 protein levels was observed in 4-HC treated cells compared with those in the control group treated with DMSO. Cells treated with 4-HC also exhibited a significant reduction in P62 protein levels. Furthermore, pre-exposure to UCMSC-derived EV-C partially attenuated the effects of 4-HC treatment on autophagy, but these changes were not statistically significant. Notably, pre-exposure to EV-H significantly mitigated the increase in the LC3-II and beclin-1 protein expression levels induced by 4-HC treatment and significantly increased P62 expression levels. These results aligned with the present *in vivo* findings which established that EV-H proficiently inhibits CP-induced autophagy activation.

Following JC-10 staining flow cytometry and microplate reader analyses were used to assess the mitochondrial membrane potential of KGN cells subjected to different treatments (Fig. 6C and D). Changes in the red/green fluorescence intensity ratio of cell samples indicated mitochondrial depolarization, with a significant decrease in mitochondrial membrane potential being observed after 4-HC treatment compared with controls. Pre-treatment with EV-H resulted in a notable shift from primarily green- to red-fluorescence emissions compared with 4-HC-treated cells, suggesting that pre-treated cells exhibited greater mitochondrial membrane potential. This was supported by the significant increase in aggregate/monomer ratio observed in 4-HC + EV-H cells compared with 4-HC cell samples. To further support these observations, the present study analyzed KGN cells via transmission electron microscopy, which represents the benchmark method for investigating autophagy (Fig. 6E). Compared with the control group, the number of mitophagic vacuoles notably increased in 4-HC-treated cells. However, compared with the 4-HC group, the number of mitophagic vacuoles markedly decreased in the EV-H pre-treatment group. These findings indicated that EV-H pre-treatment effectively protected KGN cells against 4-HC-induced damage.

Discussion

The clinical management of DOR remains a notable challenge in reproductive medicine, particularly in cases involving chemotherapy-induced premature ovarian insufficiency (35). Hyperin, a notable flavonol glycoside used in traditional Chinese medicine (TCM), has long been recognized for its potent antioxidant, anti-apoptotic and reproductive-protective properties (36-38). However, when administered via conventional OA, the therapeutic efficacy of free hyperin was notably compromised; this was potentially due to its rapid gastrointestinal degradation and notable hepatic first-pass metabolism, and consequently, its low bioavailability in target ovarian tissue (39). To circumvent these pharmacokinetic limitations, the present study successfully engineered a novel nanomedicine delivery system by encapsulating hyperin into human UCMSC-derived exosomes via ultrasonication, thereby yielding a stable and efficient hyperin formulation. The findings of the present study demonstrated that EV-H markedly outperformed therapies involving free hyperin in restoring hormone balance, preserving follicular reserves and mitigating GC injury, thereby offering a promising exosome-based strategy for DOR therapy.

The key to understanding the occurrence and development of DOR lies in establishing animal models that mimic its pathological mechanisms. Animal models of DOR established using various DOR induction methods, such as chemotherapy and drug-induced damage, have provided a solid experimental foundation for research (39-41). The chemotherapy drug CP is commonly used to induce DOR and establish DOR animal models due to its ability to notably damage ovarian function in mice and replicate the pathological characteristics of DOR (40). As such, CP-based models facilitate a more comprehensive investigation of treatment efficacy in DOR and further elucidate the corresponding mechanisms of action for such treatments than other DOR models. In the present study, a DOR mouse model was established via the intraperitoneal administration of CP at a dose of 100 mg/kg weekly for 3 consecutive weeks. Over time, DOR model mice exhibited progressively disrupted estrous cycles, which eventually stagnated in the diestrus phase. Following CP treatment, mice in the model group demonstrated markedly reduced serum AMH levels, elevated FSH levels, decreased ovarian index values, a depleted primordial follicle pool and a significantly increased incidence of follicular atresia, as well as increased conception time. All of these observations were consistent with the clinical symptoms of DOR, indicating successful modeling (41,42).

Mechanistically, the maintenance of ovarian homeostasis is intricately linked to the precise regulation of autophagy in GCs. Autophagy fundamentally plays dual roles in reproductive toxicology (43,44). Under physiological baseline conditions or mild cellular stress, autophagy acts as a pro-survival, homeostatic mechanism aimed at recycling damaged organelles and clearing reactive oxygen species (ROS) (45). However, chemotherapy with alkylating agents, such as CP, triggers an influx of intracellular ROS and results in notable amounts of double-stranded DNA breaks within GCs (46). Under such notable and chronic toxic stress, the autophagic flux shifts from a beneficial, restorative response into an unchecked, cytotoxic pathway that directly executes GC apoptosis and accelerates follicular atresia (47,48). Notably, treatment with EV-H significantly mitigated these alterations, partially restoring the expression levels of LC3-II, beclin-1 and P62 towards their respective baseline levels. Rather than completely suppressing an important physiological process, EV-H acted as a therapeutic modulator that mitigated the underlying cellular stress, as evidenced by the restoration of the mitochondrial membrane potential in KGN cells following EV-H treatment, thereby rescuing GCs from entering the cytotoxic autophagic cascade.

The present study highlighted the potential of integrating TCM with exosome technology for the treatment of DOR, utilizing exosomes derived from UCMSCs for hyperin delivery, and observed a notable protective effect on ovarian-reserve function in mice. Exosomes are natural extracellular vesicles that are widely distributed in the body and possess intrinsic therapeutic advantages, such as non-immunogenicity and easy cell membrane penetration (49). In previous years, research on exosome-based

drug delivery has expanded, demonstrating promising applications for treating various challenging diseases and tumors by successfully loading small-molecule chemical drugs and nucleic acid therapeutics into exosomes (50,51). The difference in administration routes between the OA group, which was subject to intragastric administration, and the exosome groups, which received hyperin via intraperitoneal injection, represents a notable pharmacokinetic variable. However, because EV-H treatment displayed markedly improved efficacy in restoring follicle counts and hormone profiles than empty EV-C administered via the same administration route, the present study demonstrated that the therapeutic benefits observed in the EV-H group were driven by hyperin encapsulation rather than route-dependent bioavailability alone. Compared with direct gavage and other drug-administration methods reported in literature (26,52), utilizing exosomes as drug carriers notably enhanced the targeted delivery and therapeutic bioefficacy of hyperin *in vivo*, thereby improving its therapeutic efficacy and minimizing the adverse effects associated with direct hyperin administration.

In conclusion, the present study demonstrated that hyperin-loaded exosomes exhibited notable therapeutic potential for the treatment of DOR. By integrating TCM principles with modern scientific methodologies, the present study represented a comprehensive investigation into the mechanisms by which TCM could support DOR treatment, offering more effective and safer therapeutic options for affected patients. These findings will markedly contribute toward therapies supporting female reproductive health. However, it is important to consider individual variations in treatment response and assess the long-term effectiveness of the treatment method established in the present study. Therefore, the present study presented an integrated therapeutic approach that combined TCM with modern biotechnology and offered innovative prospects for future clinical DOR treatments.

Acknowledgements

The authors would like to express their sincere gratitude to Miss Xin Pan (Key Laboratory of Cell-Based Drug and Applied Technology Development in Zhejiang Province (Hangzhou, China) for administrative support and coordination in laboratory animal management and compliance during the present study.

Funding

The present study was supported by the Zhejiang Provincial Medical and Health Science and Technology Project (grant no. 2025KY476) and the Key Technologies R&D Program of Zhejiang Province (grant nos. 2019C03041 and 2021C03077).

Availability of data and materials

The data generated in the present study may be requested from the corresponding author.

Authors' contributions

YY and YWu were responsible for performing the experiments and writing the original draft of the manuscript. JZ and YWa assisted with the experiments and analyzed the data. HY contributed toward data interpretation. GL performed animal experiments. RP and LL contributed toward conceptualization, reviewing and editing the manuscript, supervision and project management. All authors read and approved the final version of the manuscript. YY and YWu confirm the authenticity of all the raw data.

Ethics approval and consent to participate

All experimental procedures were performed according to the National Institutes of Health Guidelines for the Care and Use of Laboratory Animals and approved by the Medical Animal Experiment Ethics Committee of the Hangzhou Medical College Laboratory Animal Center, otherwise known as the Zhejiang Center of Laboratory Animals (approval no. ZJCLA-IACUC-20050016).

Patient consent for publication

Not applicable.

Competing interests

The authors declare that they have no competing interests.

References

1. Broekmans FJ, Soules MR and Fauser BC: Ovarian aging: Mechanisms and clinical consequences. Endocr Rev 30: 465-493, 2009.
2. Park SU, Walsh L and Berkowitz KM: Mechanisms of ovarian aging. Reproduction 162: R19-R33, 2021.
3. Chon SJ, Umair Z and Yoon MS: Premature ovarian insufficiency: Past, present, and future. Front Cell Dev Biol 9: 672890, 2021.
4. Scantamburlo VM, Linsingen RV, Centa LJR, Toso KFD, Scaraboto D, Araujo Júnior E and Kulak Junior J: Association between decreased ovarian reserve and poor oocyte quality. Obstet Gynecol Sci 64: 532-539, 2021.
5. Yao LN, Lin WQ, Jiang N, Li C, Cao HF, Li H and Qian JH: Comparative study of assisted reproductive outcomes between young patients with occult premature ovarian insufficiency and advanced-age patients. J Int Med Res 48: 300060520934656, 2020.
6. Abrahami N, Izhaki I and Younis JS: Do young women with unexplained infertility show manifestations of decreased ovarian reserve? J Assist Reprod Genet 36: 1143-1152, 2019.
7. Liu T, Li Q, Wang S, Chen C and Zheng J: Transplantation of ovarian granulosa-like cells derived from human induced pluripotent stem cells for the treatment of murine premature ovarian failure. Mol Med Rep 13: 5053-5058, 2016.
8. Xie Z, Li Y, Chen Z, Cao Q, Zhang C, Fei Y, Li K and Guan Y: Effects of Bushen Huoxue method for female with decreased ovarian reserve: A protocol for systematic review and meta-analysis. Medicine (Baltimore) 99: e22957, 2020.
9. Lv Z, Lv Z, Song L, Zhang Q and Zhu S: Role of lncRNAs in the pathogenic mechanism of human decreased ovarian reserve. Front Genet 14: 1056061, 2023.
10. Fusco F, Paciolla M, Chen E, Li X, Genesio R, Conti A, Jones J, Poeta L, Lioi MB, Ursini MV and Miano MG: Genetic and molecular analysis of a new unbalanced X;18 rearrangement: Localization of the diminished ovarian reserve disease locus in the distal Xq POF1 region. Hum Reprod 26: 3186-3196, 2011.
11. Ferder IC, Espeche LD, Bruque CD, Parborell F, Tesone M and Dain L: Expression and characterisation of Fmrl splice variants during folliculogenesis in the rat. Reprod Fertil Dev 34: 1034-1042, 2022.
12. Paulini F and Melo EO: The role of oocyte-secreted factors GDF9 and BMP15 in follicular development and oogenesis. Reprod Domest Anim 46: 354-361, 2011.

13. Wu W, Han J, Cao R, Zhang J, Li B, Liu Z, Liu K, Li Q, Pan Z, Chen J and Liu H: Sequence and regulation of the porcine FSHR gene promoter. Anim Reprod Sci 154: 95-104, 2015.
14. Gogola J, Hoffmann M and Ptak A: Persistent endocrine-disrupting chemicals found in human follicular fluid stimulate the proliferation of granulosa tumor spheroids via GPR30 and IGF1R but not via the classic estrogen receptors. Chemosphere 217: 100-110, 2019.
15. Henes M, Froeschlin J, Taran FA, Brucker S, Rall KK, Xenitidis T, Igney-Oertel A, Lawrenz B and Henes JC: Ovarian reserve alterations in premenopausal women with chronic inflammatory rheumatic diseases: Impact of rheumatoid arthritis, Behcet's disease and spondyloarthritis on anti-Mullerian hormone levels. Rheumatology (Oxford) 54: 1709-1712, 2015.
16. Chen J, Wu S, Wang M, Zhang H and Cui M: A review of autoimmunity and immune profiles in patients with primary ovarian insufficiency. Medicine (Baltimore) 101: e32500, 2022.
17. Kim Y, Lee E, Song JY, Kim Y and Lee S: Association between environmental pollutants and the FSH/AMH ratio as a marker of ovarian reserve. Environ Anal Health Toxicol 37: e2022029-0, 2022.
18. Osmanlioglu S, Berker B, Aslan B, Şükür YE, Özmen B, Sönmezer M, Atabekoğlu CS and Aytaç R: Presence of endometrioma does not impair embryo quality and assisted reproductive technology (ART) cycle outcome in diminished ovarian reserve (DOR) patients. Reprod Sci 30: 1540-1547, 2023.
19. Vigneswaran K and Hamoda H: Hormone replacement therapy-Current recommendations. Best Pract Res Clin Obstet Gynaecol 81: 8-21, 2022.
20. Gonda KJ, Domar AD, Gleicher N and Marrs RP: Insights from clinical experience in treating IVF poor responders. Reprod Biomed Online 36: 12-19, 2018.
21. Monteiro CS, Scheffer BB, Carvalho RF and Scheffer JB: The impact of dehydroepiandrosterone in poor ovarian responders on assisted reproduction technology treatment. JBRA Assist Reprod 23: 414-417, 2019.
22. Pellicer N, Cozzolino M, Diaz-Garcia C, Galliano D, Cobo A, Pellicer A and Herraiz S: Ovarian rescue in women with premature ovarian insufficiency: Facts and fiction. Reprod Biomed Online 46: 543-565, 2023.
23. Chen H, Liu C, Zhu S, Li S, Zhang Q, Song L and Liang X: The therapeutic effect of stem cells on Chemotherapy-Induced premature ovarian failure. Curr Mol Med 21: 376-384, 2021.
24. Wu JJ, Zhang J, Xia CY, Ding K, Li XX, Pan XG, Xu JK, He J and Zhang WK: Hypericin: A natural anthraquinone as promising therapeutic agent. Phytomedicine 111: 154654, 2023.
25. Wang X, Fan G, Wei F, Bu Y and Huang W: Hyperoside protects rat ovarian granulosa cells against hydrogen peroxide-induced injury by sonic hedgehog signaling pathway. Chem Biol Interact 310: 108759, 2019.
26. Zhu F, Gao J, Zeng F, Lai Y, Ruan X and Deng G: Hyperoside protects against cyclophosphamide induced ovarian damage and reduced fertility by suppressing HIF-1alpha/BNIP3-mediated autophagy. Biomed Pharmacother 156: 113743, 2022.
27. You F, Cao J, Cheng L, Liu X and Zeng L: Hyperin alleviates Triptolide-induced ovarian granulosa cell injury by regulating AKT/TSC1/mTORC1 signaling. Evid Based Complement Alternat Med 2021: 9399261, 2021.
28. Pan W, Gu L, Yang H, Xu C, Yang Z, Lu Q, Shi Y, Zhang L, Shao J, Chen Y, *et al*: Repeat-dose toxicity study of human umbilical cord mesenchymal stem cells in cynomolgus monkeys by intravenous and subcutaneous injection. Front Cell Dev Biol 11: 1273723, 2023.
29. Dominici M, Le Blanc K, Mueller I, Slaper-Cortenbach I, Marini F, Krause D, Deans R, Keating A, Prockop DJ and Horwitz E: Minimal criteria for defining multipotent mesenchymal stromal cells. The International Society for Cellular Therapy position statement. Cytotherapy 8: 315-317, 2006.
30. Council NR: Guide for the Care and Use of Laboratory Animals: Eighth Edition. Washington, DC, The National Academies Press, 2011.
31. Huang C, Song K, Ma W, Ding J, Chen Z and Zhang M: Immunomodulatory mechanism of Bushen Huoxue Recipe alleviates cyclophosphamide-induced diminished ovarian reserve in mouse model. J Ethnopharmacol 208: 44-56, 2017.
32. Byers SL, Wiles MV, Dunn SL and Taft RA: Mouse estrous cycle identification tool and images. PLoS One 7: e35538, 2012.
33. Ajayi AF and Akhigbe RE: Staging of the estrous cycle and induction of estrus in experimental rodents: An update. Fertil Res Pract 6: 5, 2020.
34. Chen Q, Chen Q, Song Y, Xiang Y, Li Q, Sang Y, Zhang L, Bai L and Zhu Y: Downregulation of homeobox A1 in human granulosa cells is involved in diminished ovarian reserve through promoting cell apoptosis and mitochondrial dysfunction. Mol Cell Endocrinol 580: 112084, 2024.
35. Cedars MI: Managing poor ovarian response in the patient with diminished ovarian reserve. Fertil Steril 117: 655-656, 2022.
36. Wierman ME and Kiseljak-Vassiliades K: Should dehydroepiandrosterone be administered to Women? J Clin Endocrinol Metab 107: 1679-1685, 2022.
37. Somigliana E, Li Piani L, Paffoni A, Salmeri N, Orsi M, Benaglia L, Vercellini P and Vigano' P: Endometriosis and IVF treatment outcomes: Unpacking the process. Reprod Biol Endocrinol 21: 107, 2023.
38. Zhang C and Xu X: Advancement in the treatment of diminished ovarian reserve by traditional Chinese and Western medicine. Exp Ther Med 11: 1173-1176, 2016.
39. Buigues A, Marchante M, Herraiz S and Pellicer A: Diminished ovarian reserve Chemotherapy-induced mouse model: A tool for the preclinical assessment of new therapies for ovarian damage. Reprod Sci 27: 1609-1619, 2020.
40. He R, Fan Q, Li Y, Zhu Q, Hu D, Du J, Xing Y, Li H, Liang X and Yang Y: Identification of common and specific genes involved in mouse models of Age-related and Cyclophosphamide-Induced diminished ovarian reserve. Reprod Sci 30: 1965-1978, 2023.
41. Bunnewell SJ, Honess ER, Karia AM, Keay SD, Al Wattar BH and Quenby S: Diminished ovarian reserve in recurrent pregnancy loss: A systematic review and meta-analysis. Fertil Steril 113: 818-827.e3, 2020.
42. Kučera M, Štěpán Ml J and Štelcl M: Possibilities and real meaning of assessment of ovarian reserve. Ceska Gynekol 83: 307-311, 2018.
43. Chhabra V, Meenakshi S, Maity S, Saini D, Saini M, Murti K and Kumar N: Impact of fluoride exposure on reproductive health: Insights into molecular mechanisms and health implications. Reprod Toxicol 135: 108907, 2025.
44. Nazeerulla F, Banerjee I, Paul MK, Bisht B, Basu D, Bhutia SK and Mukhopadhyay S: Autophagy as an architect of embryogenesis: Understanding the new mechanisms, emerging paradigms, and future directions. Life Sci 391: 124277, 2026.
45. Debnath J, Gammoh N and Ryan KM: Autophagy and autophagy-related pathways in cancer. Nat Rev Mol Cell Biol 24: 560-575, 2023.
46. Kawano M, McKey J, Batchvarov IS and Capel B: Granulosa cell death is a significant contributor to DNA-damaging chemotherapy-induced ovarian insufficiencydagger. Biol Reprod 112: 906-915, 2025.
47. Zhu F, Hu C, Huang S, Cao X, Li X, Song Y, Chen M and Xiao J: Qilin Pills protect against diminished ovarian reserve by suppressing pathological overactivation of PINK1/Parkin-mediated mitophagy in granulosa cells. J Ethnopharmacol 369: 121862, 2026.
48. Chen L, Zeng L, Pan S, Zu L, Pan H and Fan L: β-sitosterol in Yijing Hugui decoction prevents cyclophosphamide-induced premature ovarian insufficiency via the AKT1/Nrf2 pathway. Cytotechnology 77: 76, 2025.
49. Kalluri R and LeBleu VS: The biology, function, and biomedical applications of exosomes. Science 367: eaau6977, 2020.
50. Kimiz-Gebologlu I and Oncel SS: Exosomes: Large-scale production, isolation, drug loading efficiency, and biodistribution and uptake. J Control Release 347: 533-543, 2022.
51. Liang Y, Duan L, Lu J and Xia J: Engineering exosomes for targeted drug delivery. Theranostics 11: 3183-3195, 2021.
52. Zhou Q, Tang H, Wang Y, Hua Y, Ouyang X and Li L: Hyperoside mitigates PCOS-associated adipogenesis and insulin resistance by regulating NCOA2-mediated PPAR-gamma ubiquitination and degradation. Life Sci 364: 123417, 2025.